Enhanced Electrical Properties of Reduced Graphene Oxide Multilayer Films by *In-Situ* Insertion of a TiO_2 Layer

Joong Tark Han,[†] Beom Joon Kim,[‡] Bo Gyeong Kim,[†] Jun Suk Kim,[†] Bo Hwa Jeong,[†] Seung Yol Jeong,[†] Hee Jin Jeong,[†] Jeong Ho Cho,[‡,*] and Geon-Woong Lee[†,*]

[†]Nano Carbon Materials Research Group, Korea Electrotechnology Research Institute, Changwon, 641-120, Korea and, [‡]Department of Organic Materials and Fiber Engineering, Soongsil University, Seoul 156-743, Korea

ABSTRACT

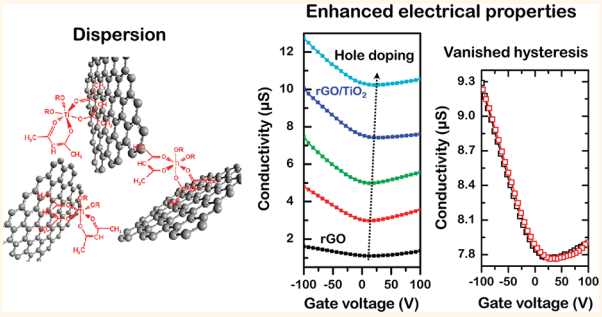

Wrinkle-free reduced graphene oxide (rGO)/TiO_2 hybrid multilayer films were directly fabricated using an rGO solution stabilized by a TiO_2 precursor sol applied over a large area by an air spraying method without the use of additional reduction processes. *In-situ* insertion of the TiO_2 layer between rGO sheets dramatically increased the conductivity and carrier mobility despite the insulating properties of amorphous TiO_2. The TiO_2 situated between rGO sheets also induced significant hole doping. Electrical hysteresis caused by adsorbed water molecules and residual oxidative moieties in the rGO nanosheets vanished due to TiO_2-assisted screening of charged impurities. These effects decreased the thermal carrier activation energy and increased the density of states at the Fermi level. Ambipolar transport properties were converted into unipolar-like hole transport characteristics by extensive hole doping in the TiO_2 layer.

KEYWORDS: reduced graphene oxide · dispersion · TiO_2 layer · conductivity · mobility · hysteresis · doping

Chemically exfoliated graphene sheets show promise for use in high-performance electronics and sensor applications because they are solution processable and display unique electrical properties.[1−9] The solution processability of graphene oxide (GO) permits application of GO to substrates *via* spin-coating, spray-casting, drop-casting, or inkjet printing for the large-scale production of graphene electronic circuits. Subsequent reduction of GO sheets can proceed through deoxygenation by thermal or by chemical reduction. The direct fabrication of uniformly reduced GO (rGO) films is difficult because rGO sheets are not easily dispersed in solvents, and they form wrinkled structures during spin-coating, spraying, or printing. Thus, the solution processability of rGO solution is most important for its application in printed electronics because we can exclude the post-reduction process considering the cost.

In this work, we present a straightforward method for addressing the problems associated with dispersing rGO nanosheets in organic solvents by introducing stabilizing hydrophobic interfacial interactions between the rGO surfaces and an acetylacetone (acac) stabilizer in a TiO_2 precursor solution. Wrinkle-free rGO/TiO_2 hybrid multilayer films were successfully fabricated by air spraying onto large substrates.

The carrier mobility and conductivity of the rGO thin films were much lower than those of mechanically cleaved graphene and CVD-grown graphene.[4−11] Any of several causes may account for the poor performance of rGO films. Chemically reduced GO include oxidative moieties such as epoxy or hydroxyl groups in the basal plane and carbonyl or carboxylic acid groups at the edges.[4,12−14] Defects created after the removal of C−O functional groups can prevent the recovery of charge transport properties to the levels seen in pristine graphene. The sheet-to-sheet junction resistance in rGO films decreases the conductivity of multilayered graphene films.[15] Conventionally, the electrical properties of reduced graphene oxide have been modified by chemical or

* Address correspondence to jhcho94@ssu.ac.kr, gwleephd@keri.re.kr.

Received for review August 10, 2011 and accepted October 23, 2011.

Published online October 23, 2011
10.1021/nn203054t

thermal reduction processes or by increasing the sheet size to reduce the sheet-to-sheet junction resistance.[8] The charge mobility of graphene sheets in direct contact with low-k oxide layers, for example, SiO_2, is much lower than the charge mobility in pure graphene due to impurity scattering from the SiO_2 substrate, which results in hysteresis.[16] Thus, the screening of charged impurities by applying high ionic strength solutions or high dielectric constant liquids can enhance charge mobility in graphene films.[8,17,18]

Titanium dioxide is a promising charge screening candidate because TiO_2 can interact electrostatically with oxygen moieties causing charge trapping,[19,20] and it has been used as an electron transporting layer or an optical spacer in organic solar cells and polymer light-emitting diodes.[21−24] The incorporation of TiO_2 layers into rGO films may prevent moisture from permeating rGO films in electronic devices.[25,26] Titania has been used previously to prepare GO/TiO_2 nanoparticle hybrid materials for photocatalytic and photoconduction applications,[19,27] although TiO_2 has not been used to enhance the electrical properties of multilayered rGO films.

Here, we report a reproducible and facile method for enhancing the carrier mobility and conductivity of rGO multilayer films at zero gate voltage by *in situ* insertion of a TiO_2 layer. The mechanism by which the electrical properties of multilayered rGO/TiO_2 films were enhanced was investigated by measuring the films' electrical properties in vacuum as a function of temperature and by observation hysteresis in the transfer curves. The ambipolar transistor properties of the rGO multilayer film were converted into unipolar properties by extensive hole doping in the TiO_2 layer.

This strategy provides several advantages: (i) TiO_2 precursor sols can stabilize rGO sheet dispersions in organic solvents by introducing hydrophobic interactions between the reduced sp^2 carbon sites and acac molecules in the TiO_2 precursor sol; (ii) the TiO_2 stabilized rGO solutions show good solution processability, resulting in formation of wrinkle-free graphene films; (iii) the charge transport properties in rGO multilayer films improve due to the charge trap screening and doping effects of a very thin TiO_2 layer, as demonstrated by the absence of hysteresis, a reduced thermal carrier activation energy, and an increased density of states at the Fermi level based on a variable range hopping (VRH) charge transport model; (iv) unipolar-like graphene transistor behavior is favored by the hole doping effects.

RESULTS AND DISCUSSION

Graphite oxide was prepared by the modified Hummer's method with pure graphite. Graphite oxide was exfoliated into GO nanosheets in dimethylformamide (DMF) by bath sonication for 30 min. Small GO nanosheets with carboxylic acid groups were removed by centrifuging the GO solution, because these nanosheets are hygroscopic and the carboxylic acid groups in the GO sheets are difficult to reduce.[28] The average size of the purified GO was several micrometers (Supporting Information, Figure S1a). GO nanosheets in solution were reduced with hydrazine by dropping hydrazine monohydrate (N_2H_4) into a GO dispersion in DMF with stirring at a concentration of 4 mM at 80 °C for 16 h. The rGO sheets agglomerated and precipitated due to $\pi-\pi$ interactions between the sp^2 carbons of an rGO sheet after reduction. The problems associated with aggregation of the rGO sheets in organic solvents were addressed by introducing noncovalent interactions among the sp^2 carbons of the rGO sheets and the TiO_2 precursor sol, as shown in Figure 1a. The TiO_2 precursor sol was prepared from a titanium isopropoxide (TIP)/ acac stabilizer (1/5 molar ratio) solution, which was added to the GO solution. The weight ratio between graphene and TiO_2 was controlled by varying the weight ratio of GO and TIP. Hereafter, the samples are denoted as GO/TIP#, for example, a sample with 1:0.7 GO:TIP ratio is denoted GO/TIP0.7. The chemical structure of the TiO_2 precursor sol was characterized by Fourier transform infrared (FTIR) spectroscopy (Supporting Information, Figure S2). An absorption band at 620 cm^{-1} was assigned to the stretching vibrations ν (Ti−O−*i*Pr) and showed that unreacted isopropoxide groups remained. Absorption bands at 660, 1030, 1425, and 1525 cm^{-1} were attributed to stretching modes of the Ti−O bond, confirming the polymerization of TIP and TiO_2. The amount of TiO_2 precursor sol added to the GO solution prior to hydrazine reduction was varied to minimize the quantity of TiO_2 precursor sol required for rGO dispersal. The weight ratio between GO and TIP in the precursor TiO_2 sol was varied between 0 and 1.5. We found that a 0.1 weight ratio of GO to TIP was the minimum requirement for stabilizing an rGO solution in DMF. Figure 1b shows that the UV absorbance of the GO/TiO_2 precursor sol solution increased during hydrazine reduction in the presence of the TiO_2 precursor sol, and precipitation was not observed. This strategy enabled us to directly deposit rGO/TiO_2 multilayer films by air spraying over a large area onto a desired substrate without the need for additional reduction procedures. Most rGO films reported previously were fabricated by spin-coating a GO solution followed by thermal or chemical reduction at elevated temperatures because of the poor solution processability of rGO solutions, resulting in wrinkled structures, as shown in Supporting Information, Figure S3.

We fabricated rGO/TiO_2 hybrid multilayer films on SiO_2 surfaces by automatic spray-coating of the stabilized rGO solution, and the prepared films were heated at 200 °C for 1 h to remove the acac TiO_2 sol stabilizer.

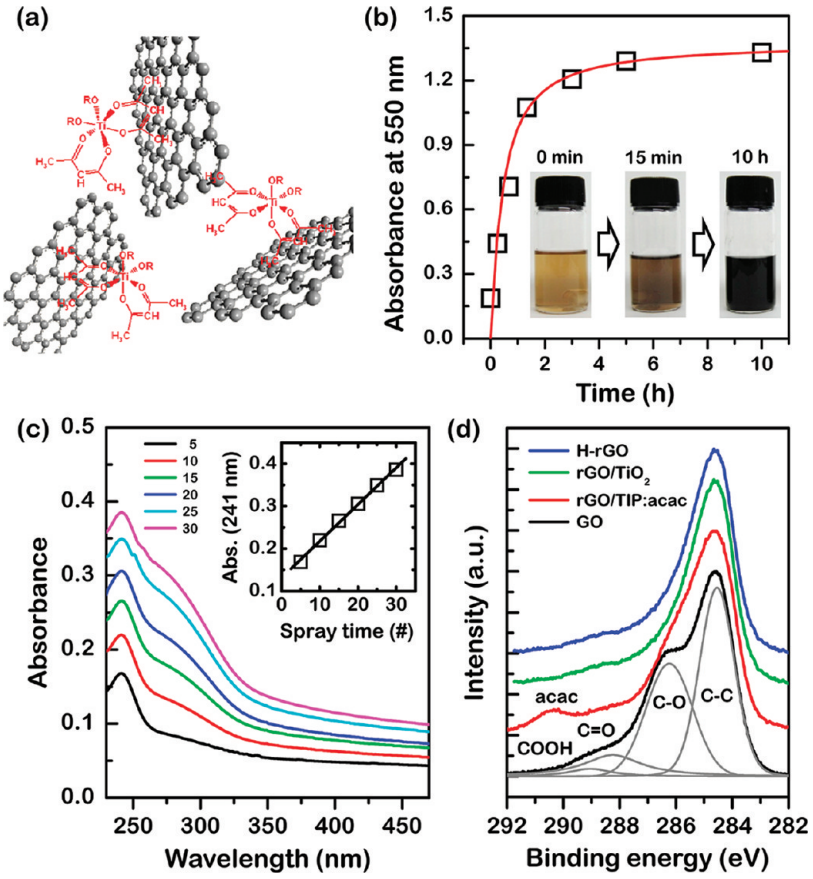

Figure 1. (a) Proposed mechanism by which the rGO sheets are dispersed in the presence of the TiO_2 precursor sol. (b) Absorbance of the GO solution at 550 nm during reduction with hydrazine monohydrate. The inset images in panel b show vials containing the GO solution as a function of the reduction time. (c) UV−vis absorption spectra of the rGO/TiO_2 hybrid multilayer films, and plot showing the linear relationship between the absorbance at 241 nm and the number of spraying applications. (d) XPS C1s spectra of GO, rGO reduced by hydrazine vapor (H-rGO), rGO/TIP:acac (before thermal treatment), and rGO/TiO_2 (after thermal treatment at 200 °C) films.

The rGO multilayer films prepared without a TiO_2 layer were prepared by reducing the GO films prepared by spraying with hydrazine vapor at 100 °C. The straightforward build-up of rGO/TiO_2 hybrid multilayer films by air spraying was monitored by UV−vis absorption spectroscopy. A higher absorption cross-section was assigned to the cumulative layering of rGO and TiO_2 layers, as shown in Figure 1c. The linear increase in the peak absorbance at 241 nm with the number of rGO/TiO_2 solution spray applications, as shown in the inset of Figure 1c, indicates that the deposition was uniform. The total thickness of the films increased upon addition of the TiO_2 precursor sol, so the number of GO layers was held constant by fixing the transmittance of the films deposited on glass substrates at 87%. Atomic force microscopy (AFM) images, as shown in Supporting Information, Figure S1b, show that the total film thickness of the rGO films without TiO_2 was several nanometers, which indicated the preparation of continuous few-layer rGO films.

Figure 1d shows an X-ray photoelectron spectroscopy (XPS) analysis of GO, rGO, rGO/TiO_2 precursor sol, and rGO/TiO_2 multilayer films, which indicates that the oxidative groups were reduced by hydrazine reduction and the acac molecules stabilized the TiO_2 sol in films prior to thermal treatment at 200 °C. Importantly, reduction of the GO sheets by hydrazine in solution was not influenced by the presence of the TiO_2 precursor sol. The presence of TiO_2 in the rGO hybrid films was confirmed by XPS, as shown in Supporting Information, Figure S4. The Ti2p XPS peaks at 459.6 and 465.4 eV were attributed to TiO_2. Figure 2 panels a−c show the surface morphologies of rGO/TiO_2 films by AFM. The rGO/TIP0.2 film did not form a continuous TiO_2 layer because the concentration of the TiO_2 precursor sol was too low, whereas in rGO/TIP0.5, the rGO surfaces were fully covered with a TiO_2 layer. A scanning electron microscopy (SEM) image in Figure 2d clearly revealed a flat rGO film hybridized with TiO_2 in contrast with wrinkled structures of rGO nanosheets reduced in DMF solvothermally without TiO_2 layer (Supporting Information, Figure S3). The top view morphologies of the rGO/TIP0.5 and rGO/TIP1.2 films did not differ in the SEM and AFM images, which suggests that only the TiO_2 layer thickness increased upon further additions of the TiO_2

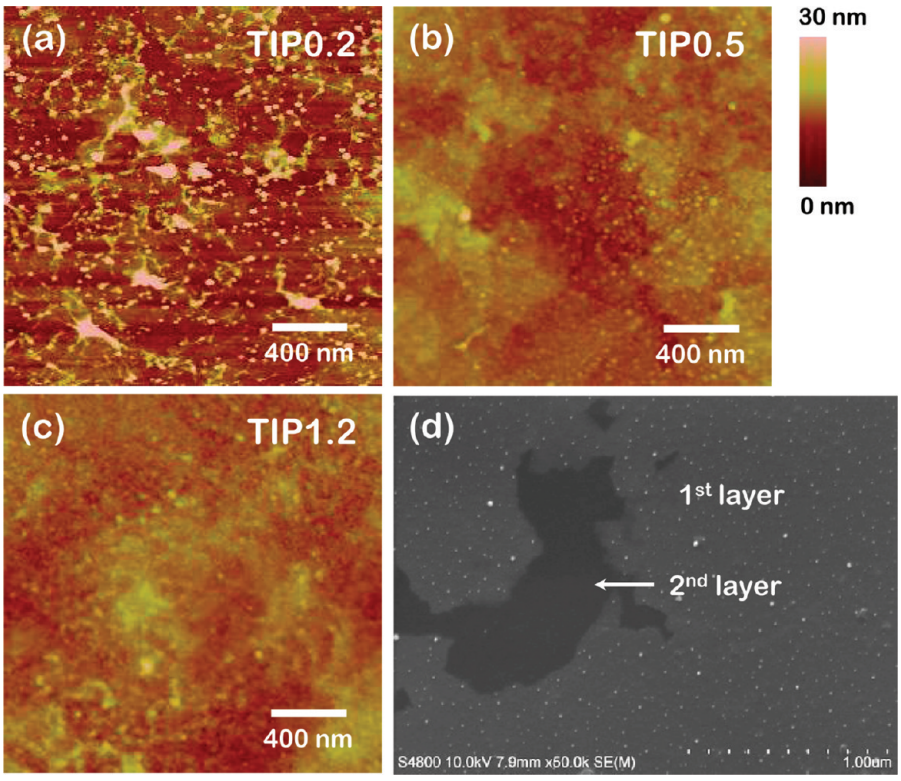

Figure 2. AFM images of rGO/TIP (a) 0.2, (b) 0.5, and (c) 1.2. (d) SEM image of an rGO/TIP 0.7 film.

precursor sol. The increased thickness of single-layered rGO/TiO_2 hybrid nanosheets shown in Supporting Information, Figure S5 supports this suggestion. The selective interactions between rGO and the TiO_2 precursor were also demonstrated by observing single-layered rGO/TiO_2 hybrid films, as shown in Figure S5.

The electrical transport characteristics of the rGO and rGO/TiO_2 hybrid films were investigated by preparing graphene field-effect transistors (FETs) on heavily doped Si substrates, which are commonly employed as gate electrodes. A thermally grown 285 nm thick SiO_2 layer served as the gate dielectric. Source and drain electrodes were deposited by thermal evaporation of Au (Supporting Information, Figure S6). The channel length (L) and channel width (W) were 100 and 800 μm, respectively. The hole and electron mobilities were extracted from the linear regime of the transfer characteristics measurements using the relation $\mu = (L/V_D C_i W)(dI_D/dV_G)$, where C_i is the specific capacitance of the gate dielectric (12.1 nF/cm^2). I_D, V_D (0.1 V) and V_G are the drain current, drain voltage, and gate voltage, respectively. The average mobility was calculated from more than 20 devices.

Figure 3a presents the transfer characteristics (I_D *vs* V_G) of the graphene FETs based on the rGO and rGO/TiO_2 hybrid films. The characteristic *V*-shaped ambipolar behavior, which represented both electron and hole conduction, was obtained for all devices. The hole and electron mobilities were measured to be 0.48 and 0.31 cm^2/(V s) for rGO film without a TiO_2 layer, respectively. These values were comparable to that of graphene FETs based on chemically processed few-layer graphene sheets.[4,10,11] As the TiO_2 content was increased, the hole mobility of the rGO FETs increased dramatically by as much as a factor of 9, whereas the electron mobility increased only slightly (Figure 3b). The hole and electron mobilities reached their highest values at 4.31 and 0.79 cm^2/(V s) for GO/TIP0.7 and GO/TIP0.3, respectively. It is worth noting that the conductivity of the rGO film at the charge neutral point was maximized for GO/TIP0.7 by insertion of a thin TiO_2 layer into the rGO multilayer film, despite the amorphous insulating characteristics of TiO_2. The conductivity decreased upon the addition of additional TiO_2 sol (Figure 3a). The conductivity of GO/TIP1.5 was even larger than that of the rGO film without a TiO_2 layer.

Importantly, the threshold voltages of these devices shifted by +16 V from 12 to 28 V (Figure 3d), and the asymmetry between the hole and electron mobilities increased dramatically upon addition of the TiO_2 sol. Both rGO/TIP0.5 and rGO/TIP0.7 FETs exhibited unipolar-like transport characteristics. These results indicated that the TiO_2 introduced hole doping into the rGO. Previously, Li *et al.* reported that unipolar graphene FETs could be fabricated by insertion of a titanium oxide layer beneath the metal electrode.[29] They suggested that the titanium oxide atomic layers on the graphene surface induced hole doping. Doping of the graphene sheets grown by chemical vapor deposition or mechanically cleaved graphene was monitored

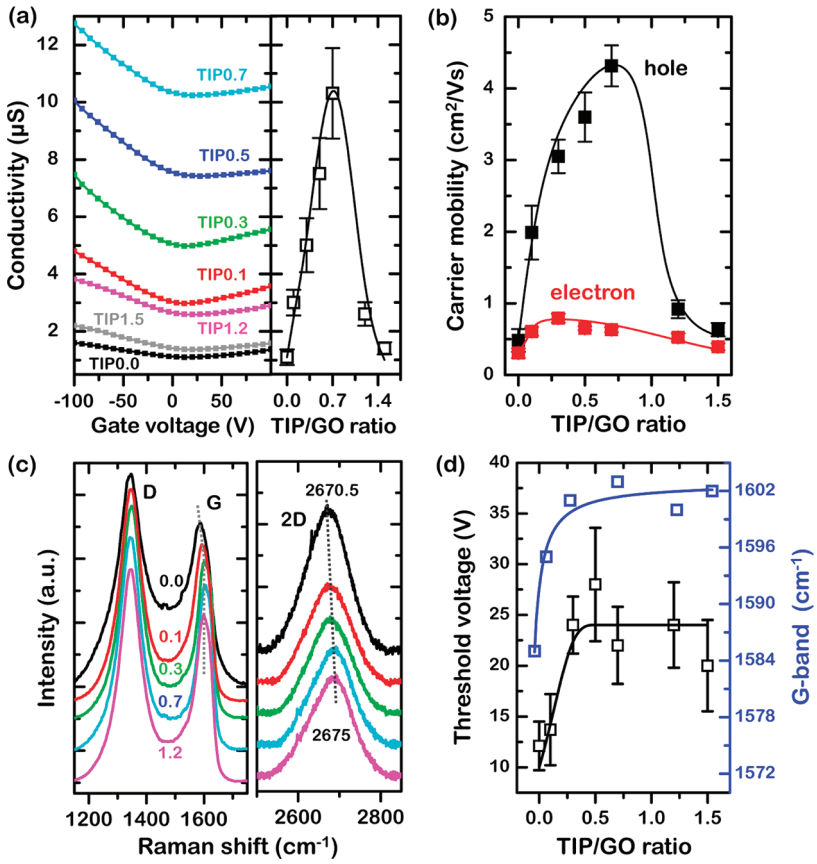

Figure 3. (a) Transfer characteristics and (b) mobility of rGO and rGO/TiO_2 hybrid multilayer films as a function of the GO/TIP ratio. (c) Raman spectra of rGO and rGO/TiO_2 hybrid multilayer films for varying amounts of TiO_2. 2D Raman spectra were magnified for easy visualization. 2D/G intensity ratios of rGO and rGO/TiO_2 hybrid films are 0.074 and 0.0598, respectively. (d) The threshold voltage of the films from the transfer curves and Raman G-bands as a function of the GO/TIP ratio.

by Raman spectroscopy.[30−33] We investigated the evolution of the Raman spectra by increasing the amount of TiO_2. The Raman spectra were excited with a 532 nm line for 10 s to avoid overheating the samples. As shown in Figure 3c, significant blue shift of the G and 2D peaks can be seen as the amount of TiO_2 increases. This may reflect that the hole doping effect strengthens with increasing TiO_2, since both hole and electron doping move the Fermi level away from the Dirac point and result in a blue-shift of the G and 2D peaks.[33]

Figure 4 shows the transfer characteristics of rGO FETs based on the rGO containing various amounts of TiO_2 during the forward and reverse V_G traces. rGO multilayer films and rGO/polymer composite films have previously displayed hysteresis, even under vacuum,[10] whereas single layer rGO sheets showed hysteresis-free back-gate-dependent conductivity under vacuum.[34] In our study, hysteresis was observed in the rGO FETs without TiO_2, even under vacuum, as shown in Figure 4a. The residual oxidative moieties and adsorbed water molecules in the rGO multilayer films, both of which may be polarized under an applied electric field, introduce a current hysteresis during the V_G sweep, due to trapping of charge carriers. Importantly, the current hysteresis gradually decreased with increasing TiO_2, and the hysteresis completely vanished in the GO/TIP0.7 FETs, unlike the behavior observed in weakly disordered graphene. We suggest that favorable interactions among TiO_2 and oxygen moieties in rGO sheets, as shown in the inset of Figure 4b, reduce carrier trapping by the polarized oxygen moieties and prevent water molecules from penetrating the rGO multilayer films.

The charge transport mechanism in rGO and rGO/TiO_2 hybrid multilayer films was investigated through temperature-dependent transport property measurements. Figure 5a shows representative transfer curves for GO/TIP0.1 FETs over the range 290−80 K. As the temperature decreased, the conductivity decreased and the on/off current ratios increased slightly. The Dirac point approached 0 V, and the *V* shape of the ambipolar characteristics became more pronounced at lower temperatures. Here, we examine the minimum conductivity σ_{min} of rGO instead of σ (V_G = 375 0 V), to exclude the effects of charged impurities. Figure 5b shows an Arrhenius plot of $\ln(\sigma_{min})$ as a function of T^{-1}, which displays several regimes with different slopes, suggesting that the density of states was not constant. The activation

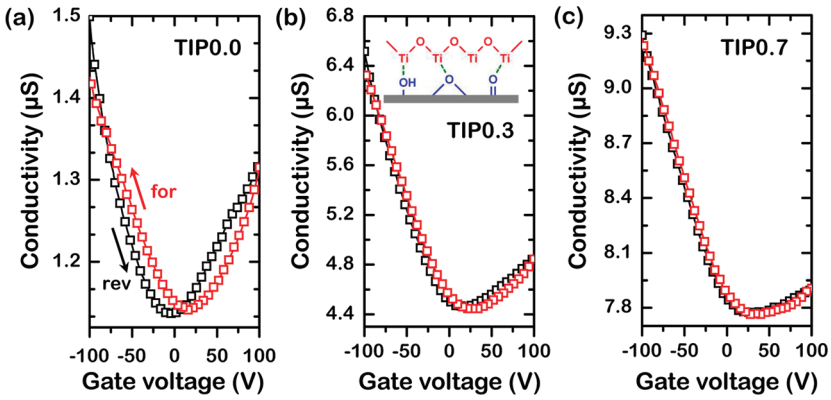

Figure 4. Reverse and forward transfer curves of (a) rGO, (b) rGO/TIP0.3, and (c) the rGO/TIP0.7 films. Inset in panel bshows possible interactions between TiO_2 and the residual oxygen moieties in the rGO films after removal of the acac molecules.

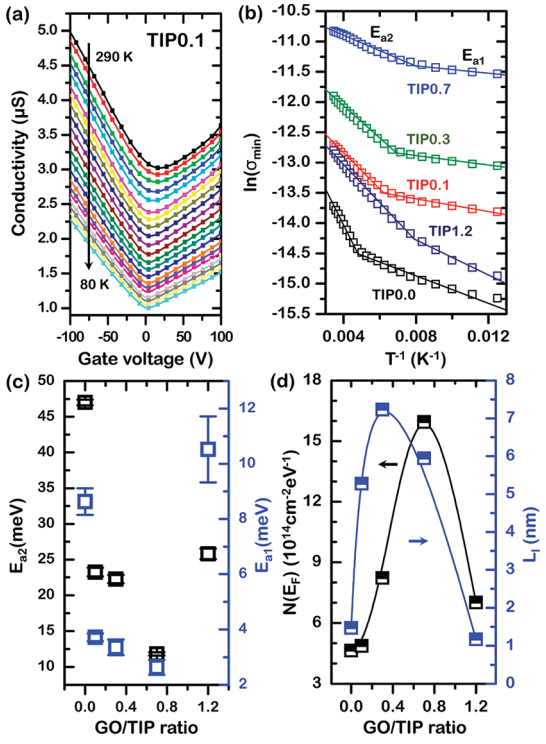

Figure 5. (a) Temperature-dependent conductivity *vs* gate voltage plots of the SiO_2-back gated graphene transistor based on an rGO/TiO_2 hybrid film; (b) ln(σ_{min}) *vs* T^{-1} plots of the graphene transistors based on rGO and rGO/TiO_2 hybrid films; (c) thermal activation energy (E_{a1} and E_{a2}) obtained from a linear fit to the Arrhenius plot; (d) density of states at the Fermi level $N(E_F)$ and localization length L_i as a function of the GO/TIP ratio.

energies E_a extracted from the low- and high-temperature regimes were designated E_{a1} and E_{a2}, respectively. As summarized in Figure 5c, both E_{a1} and E_{a2} decreased dramatically upon insertion of the TiO_2 layer. More addition of TiO_2 introduced a dielectric barrier between the semimetallic rGO sheets, which dramatically increased the activation energy. The activation energy provided a rough estimate for the total energy required for thermal carrier activation and transport in the rGO/TiO_2 hybrid films. Such anomalous behavior has been observed previously in graphene/polymer composites.[10] rGO/TiO_2 hybrid films are highly disordered systems due to intrinsic defects in rGO and randomly arranged TiO_2. Therefore, charge transport in the rGO/TiO_2 composite film was expected to require a combination of models, that is, thermal activation of charge, tunneling through TiO_2, and variable range hopping (VRH) within the rGO.[35]

The temperature-dependent conductivity of the VRH model could be described as

$$\sigma = A \exp\left(-\frac{B}{T^{1/3}}\right) \quad (1)$$

The parameter A is given by

$$A = \frac{eR_o^2 \nu_{ph}}{k_B}$$

where k_B is the Boltzmann's constant, R_o is the optimum hopping distance, and ν_{ph} is the frequency of the phonons associated with the hopping process. The hopping parameter B is given by

$$B = \left(\frac{3}{k_B N(E_F) L_l^2}\right)^{1/3}$$

where $N(E_F)$ and L_l are the density of states near the Fermi level and the localization length of the electronic wave function, respectively. Further insights into the electronic structure of rGO and rGO/TiO_2 hybrid multilayer films can be gained by investigating parameter B from the temperature-dependence of σ_{min} as the function of $T^{-1/3}$, (Figure S7a).[10,35,36]

The slope of ln(σ_{min}) *versus* $T^{-1/3}$ provided B values for devices based on the rGO and rGO/TiO_2 multilayer films. The differences in the B values could be understood from estimates of $N(E_F)$ and L_l for rGO and rGO/TiO_2 multilayer films. First, $N(E_F)$ was roughly estimated according to the equation

$$dn_i/dT = k_B N(E_F) \quad (2)$$

which is valid at temperatures near 0 K; n_i in this equation is the intrinsic carrier concentration, which can be calculated according to the relationship

$$\sigma_{max} = \sigma_{min}{}^{-1} = (en_i(\mu_h + \mu_n))^{-1} \quad (3)$$

from measurements at different temperatures. Here, ρ_{max} is the maximum resistivity, μ_h and μ_n are the hole and electron mobilities, respectively. Plots of n_i *versus* T at 100 K (Supporting Information, Figure S7b) were fit to eq 2, and the values of $N(E_F)$ for rGO and rGO/TiO_2 multilayer film transistors were estimated. These results indicated that the number of localized states near E_F that participated in charge transport was tunable by *in situ* insertion of a TiO_2 layer in the rGO multilayer film. Furthermore, the values of $N(E_F)$ and the estimated B values permitted calculation of L_l for the transistor devices (Figure 5d). These values indicated that delocalization of the charge carriers in the rGO multilayer film increased upon insertion of the TiO_2 layer. These results suggested that the activation energy decreased and the density of states increased at E_F due to p-type doping and detrapping effects with increasing TiO_2. These effects were the key factors contributing to the enhanced electrical properties of the rGO/TiO_2 hybrid multilayer films.

CONCLUSIONS

We demonstrated that TiO_2 prepared by a sol–gel process enhanced the conductivity, carrier mobility, dispersion stability, and solution processability of rGO nanosheets. A stable dispersion of rGO sheets in an organic solvent was achieved as a result of hydrophobic interactions between sp^2 carbons in rGO surfaces and acac stabilizer ligands in the TiO_2 precursor sol. The addition of TiO_2 resulted in hole doping of the rGO. The current hysteresis vanished due to a reduction in the charge trapping sites in the rGO film. The conductivity of the rGO multilayer films was therefore enhanced, and the carrier mobility could be controlled by varying the quantity of TiO_2 sol in the precursor solution. We further demonstrated that *in situ* insertion of a TiO_2 layer decreased the thermal activation barrier of the carriers and increased the density of states at E_F by hole doping effects. These results are exciting because they reaffirm the potential of solution processable rGO sheets for large-scale nanocarbon electronics.

METHODS

Graphene oxide was prepared from natural graphite (Alfa Aesar, 99.999% purity, −200 mesh) by a modified Hummers method. Briefly, 20 g of graphite and 460 mL of H_2SO_4 were mixed in a flask. Then, 60 g of $KMnO_4$ were slowly added over 1 h. Stirring was continued for 2 h in an ice–water bath. After the mixture was stirred vigorously for 18 h at room temperature, 920 mL of deionized water was added, and the solution was stirred for 10 min in an ice–water bath. Fifty milliliters of H_2O_2 (30 wt % aqueous solution) was then added, and the mixture was stirred for 2 h at room temperature. The resulting mixture was precipitated and filtered to obtain the graphite oxide powder. Graphite oxide was then exfoliated into GO nanosheets in deionized water (200 mg/L) by bath sonication for 30 min.

The TiO_2 precursor sol was prepared using TIP/acac (in a 1:5 molar ratio), ethanol, HCl, and water by stirring at 60 °C for 10 h, followed by solvent exchange with DMF. Next, the GO solution was mixed with various amounts of the TiO_2 precursor sol, and hydrazine monohydrate (N_2H_4) was added dropwise to the GO/TiO_2 precursor sol solutions to a final concentration of 4 mM, followed by heating at 100 °C for 24 h.

GO and rGO/TiO_2 hybrid films were fabricated at room temperature using an automatic spray coater (NCS Co., NCS400) with a nozzle 1.2 mm in diameter. The GO films were then reduced by heating under hydrazine fumes at 100 °C for 2 h to fabricate rGO films. The prepared rGO/TiO_2 hybrid films were heated at 200 °C to cure the TiO_2 sol and remove any remaining chemicals, such as solvents or TiO_2 sol stabilizers. Source and drain electrodes were then deposited by evaporating Au through a shadow mask. The channel length and width of a typical device were 100 and 800 μm, respectively. The transistor current–voltage characteristics were measured using Keithley 2400 and 236 source/measure units under vacuum (10^{-5} Torr). The temperature-dependent transport measurements were conducted in a cryostat (ST-500, Janis) with a base pressure of 10^{-5} Torr over the range 80–290 K.

The morphologies of the rGO and rGO/TiO_2 hybrid films were imaged by AFM (Park Systems XE-100 Multimodes), and field emission scanning electron microscopy (FE-SEM, HITACHI S4800). The absorbance of the prepared films and the GO solution during reduction were measured by UV–vis spectroscopy (Varian, Cary 5000). The structural characteristics of the RGO sheets were investigated by by confocal Raman spectrometer (NTEGRA SPECTRA, NT-MDT) with an excitation wavelength of 532 nm. To confirm the change in the carbon to oxygen atomic ratio in the functional groups of the films after reduction, XPS analysis was conducted using a Multilab2000 (Thermo VG Scientific Inc.) spectrometer with monochromatized Al Kα X-ray radiation as the X-ray excitation source.

Acknowledgment. This work was supported by a grant from the Global Frontier Research Center for Advanced Soft Electronics by the Ministry of Educational Science and Technology, Republic of Korea.

Supporting Information Available: AFM images and height profiles of the rGO films, FTIR spectra of the TiO_2 precursor sol, XPS spectra of the rGO/TiO_2 hybrid film; SEM image of a solvothermally reduced rGO film; temperature- and electric field-dependent plots for a graphene FET. This material is available free of charge *via* the Internet at http://pubs.acs.org.

REFERENCES AND NOTES

1. Stankovich, S.; Dikin, D. A.; Dommett, G. H. B.; Kohlhaas, K. M.; Zimney, E. J.; Stach, E. A.; Piner, R. D.; Nguyen, S. T.; Ruoff, R. S. Graphene-Based Composite Materials. *Nature* **2006**, *442*, 282–286.
2. Stankovich, S.; Dikin, D. A.; Piner, R. D.; Kohlhaas, K. A.; Kleinhammes, A.; Jia, Y.; Wu, Y.; Nguyen, S. T.; Ruoff, R. S. Synthesis of Graphene-Based Nanosheets *via* Chemical Reduction of Exfoliated Graphite Oxide. *Carbon* **2007**, *45*, 1558–1565.
3. Gilje, S.; Han, S.; Wang, M.; Wang, K. L.; Kaner, R. B. A Chemical Route to Graphene for Device Applications. *Nano Lett.* **2007**, *7*, 3394–3398.
4. Eda, G.; Fanchini, G.; Chhowalla, M. Large-Area Ultrathin Films of Reduced Graphene Oxide as a Transparent and Flexible Electronic Material. *Nat. Nanotechnol.* **2008**, *3*, 270–274.

5. Becerril, H. A.; Mao, J.; Liu, Z.; Stoltenberg, R. M.; Bao, Z.; Chen, Y. Reduced Graphene Oxide Films as Transparent Conductors. *ACS Nano* **2008**, *2*, 463–470.
6. Li, X.; Zhu, Y.; Cai, W.; Borysiak, M.; Han, B.; Chen, D.; Piner, R. D.; Colombo, L.; Ruoff, R. S. Transfer of Large-Area Graphene Films for High-Performance Transparent Conductive Electrodes. *Nano Lett.* **2009**, *9*, 4359–4363.
7. Zhao, J.; Pei, S.; Ren, W.; Gao, L.; Cheng, H. Efficient Preparation of Large-Area Graphene Oxide Sheets for Transparent Conductive Films. *ACS Nano* **2010**, *4*, 5245–5252.
8. Wang, S.; Ang, P. K.; Wang, Z.; Tang, A. L. L.; Thong, J. T. L.; Loh, K. P. High Mobility, Printable, and Solution-Processed Graphene Electronics. *Nano Lett.* **2010**, *10*, 92–98.
9. Jeong, S. Y.; Kim, S. H.; Han, J. T.; Jeong, H. J.; Yang, S. H.; Lee, G.-W. High Performance Transparent Conductive Films with Rheologically-Derived Reduced Graphene Oxide. *ACS Nano* **2011**, *5*, 870–878.
10. Eda, G.; Chhowalla, M. Graphene-Based Composite Thin Films for Electronics. *Nano Lett.* **2009**, *9*, 814–818.
11. Wang, S.; Chia, P.-J.; Chua, L.-L.; Zhao, L.-H.; Png, R.-Q.; Sivaramakrishnan, S.; Zhou, M.; Goh, R. G.-S.; Friend, R. H.; Wee, A. T.-S.; *et al.* Band-like Transport in Surface Functionalized Highly Solution-Processable Graphene Nanosheets. *Adv. Mater.* **2008**, *20*, 3440–3446.
12. Lerf, A.; He, H.; Forster, M.; Klinowski, J. Structure of Graphite Oxide Revisited. *J. Phys. Chem. B* **1998**, *102*, 4477–4482.
13. Szabó, T.; Berkesi, O. DRIFT Study of Deuterium-Exchanged Graphite Oxide. *Carbon* **2005**, *43*, 3186–3189.
14. Fuente, E.; Menendez, J. A.; Diez, M. A.; Suarez, D.; Montes-Moran, M. A. Infrared Spectroscopy of Carbon Materials: A Quantum Chemical Study of Model Compounds. *J. Phys. Chem. B* **2003**, *107*, 6350–6359.
15. Stankovich, S.; Piner, R. D.; Nguyen, S. T.; Ruoff, R. S. Synthesis and Exfoliation of Isocyanate-Treated Graphene Oxide Nanoplatelets. *Carbon* **2006**, *44*, 3342–3347.
16. Novikov, D. S. Numbers of Donors and Acceptors from Transport Measurements in Graphene. *Appl. Phys. Lett.* **2007**, *91*, 102102.
17. Chen, F.; Xia, J.; Tao, N. Ionic Screening of Charged-Impurity Scattering in Graphene. *Nano Lett.* **2009**, *9*, 1621–1625.
18. Kim, B. J.; Jang, H.; Lee, S.-K.; Hong, B. H.; Ahn, J.-H.; Cho, J. H. High-Performance Flexible Graphene Field Effect Transistors with Ion Gel Gate Dielectrics. *Nano Lett.* **2010**, *10*, 3464–3466.
19. Manga, K. K.; Wang, S.; Jaiswal, M.; Bao, Q.; Loh, K. P. High-Gain Graphene-Titanium Oxide Photoconductor Made from Inkjet Printable Ionic Solution. *Adv. Mater.* **2010**, *22*, 5265–5270.
20. Han, J. T.; Kim, B. G.; Yang, M.; Kim, J. S.; Jeong, H. J.; Jeong, S. Y.; Hong, S. H.; Lee, G. W. Titania-Assisted Dispersion of Carboxylated Single-Walled Carbon Nanotubes in a ZnO sol for Transparent Conducting Hybrid Films. *ACS Appl. Mater. Interfaces* **2011**, *3*, 2671–2676.
21. Arango, A. C.; Johnson, L. R.; Bliznyuk, V. N.; Schlesinger, Z.; Carter, S. A.; Hörhold, H.-H. Efficient Titanium Oxide/Conjugated Polymer Photovoltaics for Solar Energy Conversion. *Adv. Mater.* **2000**, *12*, 1689–1692.
22. Thelakkat, M.; Schmitz, C.; Schmidt, H.-W. Fully Vapor-Deposited Thin-Layer Titanium Dioxide Solar Cells. *Adv. Mater.* **2002**, *14*, 577–581.
23. Hal, P. A.; van; Wienk, M. M.; Kroon, J. M.; Verhees, W. J. H.; Slooff, L. H.; Gennip, W. J. H.; van, Jonkheijm, P.; Janssen, R. A. J. Photoinduced Electron Transfer and Photovoltaic Response of a MDMO-PPV:TiO_2 Bulk-Heterojunction. *Adv. Mater.* **2003**, *15*, 118–121.
24. Kim, J. Y.; Kim, S. H.; Lee, H.-H.; Lee, K.; Ma, W.; Gong, X. New Architecture for High-Efficiency Polymer Photovoltaic Cells using Solution-Based Titanium Oxide as an Optical spacer. *Adv. Mater.* **2006**, *18*, 572–576.
25. Cho, S.; Lee, K.; Heeger, A. J. Extended Lifetime of Organic Field-Effect Transistors Encapsulated with Titanium Sub-Oxide as an `Active' Passivation/Barrier Layer. *Adv. Mater.* **2009**, *21*, 1941–1944.
26. Lee, K.; Kim, J. Y.; Park, S. H.; Kim, S. H.; Cho, S.; Heeger, A. J. Air-Stable Polymer Electronic Devices. *Adv. Mater.* **2007**, *19*, 2445–2449.
27. Manga, K. K.; Zhou, Y.; Yan, Y.; Loh, K. P. Multilayer Hybrid Films Consisting of Alternating Graphene and Titania Nanosheets with Ultrafast Electron Transfer and Photoconversion Properties. *Adv. Mater.* **2009**, *19*, 3638–3643.
28. Han, J. T.; Kim, J. S.; Kwak, D.; Kim, B. G.; Jeong, B. H.; Jeong, S. Y.; Jeong, H. J.; Cho, K.; Lee, G. −W. Transparent Carbon Nanotube Patterns Template by Inkjet-Printed Graphene Oxide Nanosheets. *RSC Adv.* **2011**, *1*, 44–47.
29. Li, H.; Zhang, Q.; Liu, C.; Xu, S.; Gao, P. Ambipolar to Unipolar Conversion in Graphene Field-Effect Transistors. *ACS Nano* **2011**, *5*, 3198–3203.
30. Ferrari, A. C.; Meyer, J. C.; Scardaci, V.; Casiraghi, C.; Lazzeri, M.; Mauri, F.; Piscanes, S.; Jiang, D.; Novoselov, K. S.; Roth, S.; *et al*. Raman Spectrum of Graphene and Graphene Layers. *Phys. Rev. Lett.* **2006**, *97*, 187401.
31. Das, A.; Pisana, S.; Chakraborty, B.; Piscanec, S.; Saha, S. K.; Waghmare, U. V.; Novoselov, K. S.; Krishnamurthy, H. R.; Geim, A. K.; Ferrari, A. C.; *et al.* Monitoring Dopants by Raman Scattering in an Electrochemically Top-Gated Graphene Transistor. *Nat. Nanotechnol.* **2008**, *3*, 210–215.
32. Dong, X.; Fu, D.; Fang, W.; Shi, Y.; Chen, P.; Li, L.-J. Doping Single-Layer Graphene with Aromatic Molecules. *Small* **2009**, *5*, 1422–1426.
33. Malard, L. M.; Pimenta, M. A.; Dresselhaus, G.; Dresselhaus, M. S. Raman Spectroscopy in Graphene. *Phys. Rep* **2009**, *473*, 51–87.
34. Jung, I.; Dikin, D. A.; Piner, R. D.; Ruoff, R. S. Tunable Electrical Conductivity of Individual Graphene Oxide Sheets Reduced at "Low" Temperatures. *Nano Lett.* **2008**, *8*, 4283–4287.
35. Kaiser, A. B.; Gomez-Navarro, C.; Sundaram, R. S.; Burghard, M.; Kern, K. Electrical Conduction Mechanism in Chemically Derived Grpahene Monolayers. *Nano Lett.* **2009**, *9*, 1787–1792.
36. Eda, G.; Mattevi, C.; Yamaguchi, H.; Kim, H.; Chhowalla, M. Insulator to Semimetal Transition in Graphene Oxide. *J. Phys. Chem. C* **2009**, *113*, 15768–15771.